

# Calculations of Spin Fluctuation Spectral Functions $\alpha^2F$ in High-Temperature Superconducting Cuprates

Griffin Heier and Sergey Y. Savrasov

*Department of Physics, University of California, Davis, CA 95616*

(Dated: November 12, 2024)

Spin fluctuations have been proposed as a key mechanism for mediating superconductivity, particularly in high-temperature superconducting cuprates, where conventional electron-phonon interactions alone cannot account for the observed critical temperatures. Traditionally, their role has been analyzed through tight-binding based model Hamiltonians. In this work we present a method that combines density functional theory with a momentum- and frequency-dependent pairing interaction derived from the Fluctuation Exchange (FLEX) type Random Phase Approximation (FLEX-RPA) to compute Eliashberg spectral functions  $\alpha^2F(\omega)$  which are central to spin fluctuation theory of superconductivity. We apply our numerical procedure to study a series of cuprates where our extracted material specific  $\alpha^2F(\omega)$  are found to exhibit remarkable similarities characterized by a sharp peak in the vicinity of 40–60 meV and their rapid decay at higher frequencies. Our exact diagonalization of a linearized BCS gap equation extracts superconducting energy gap functions for realistic Fermi surfaces of the cuprates and predicts their symmetry to be  $d_{x^2-y^2}$  in all studied systems. Via a variation of on-site Coulomb repulsion  $U$  for the copper  $d$ -electrons we show that that the range of the experimental values of  $T_c$  can be reproduced in this approach but is extremely sensitive to the proximity of the spin density wave instability. These data highlight challenges in building first-principle theories of high temperature superconductivity but offer new insights beyond previous treatments, such as the confirmation of the usability of approximate BCS-like  $T_c$  equations, together with the evaluations of the material specific coupling constant  $\lambda$  without reliance on tight-binding approximations of their electronic structures.

PACS numbers:

## I. INTRODUCTION

Strong antiferromagnetic spin fluctuations have long been considered a potential mechanism for unconventional superconductivity, following early theoretical proposals[1, 2]. Shortly after these foundational papers the first high-temperature superconductor was discovered[3]. In spin fluctuation theory, the interaction vertex is commonly modeled using the Random Phase Approximation (RPA), which serves as a simplified representation of the true interaction vertex. Despite its simplicity, the RPA approach provides good qualitative results, particularly in capturing the divergent behavior as the spin density wave (SDW) is approached, an essential feature of many unconventional superconductors. The RPA vertex also naturally takes into account Fermi surface nesting, a phenomenon frequently observed in these systems[4]. As a result, spin fluctuations have remained a popular candidate for explaining superconductivity and have been applied extensively in the theoretical analysis of various unconventional superconductors. These materials include cuprates[5–8], nickelates[9, 10], ruthenates[11, 12], cobaltates[13], ironates[14–17], and heavy fermion[18, 19] systems.

At a given level of doping, theoretical methods typically aim to predict the onset of superconductivity, characterized by the transition temperature  $T_c$ , as well as the symmetry of the resulting superconducting gap function. Most approaches utilize simple tight-binding mod-

els with a limited number of orbitals and band structures, found using the Local Density Approximation[20] (LDA), which serve as an input to the Hubbard model Hamiltonian. The latter is subsequently solved by an available many-body technique, such, for example, as the Fluctuational Exchange Approximation (FLEX) [21]. FLEX is a diagrammatic method that includes RPA diagrams given by the particle-hole ladders and bubbles as well as particle-particle ladder diagrams. It is however known that in the vicinity of the SDW instability the most divergent terms are due to the particle-hole ladders[22, 23], and the contribution from the particle-particle ladders can be neglected[24].

Although a lot of past studies of spin fluctuational superconductivity utilized RPA and FLEX[25], the extension of this technique has been proposed recently by combining them with dynamical mean field theory (DMFT) [26]. It has resulted in reproducing doping dependence of the  $T_c$  in the simulation of the two-dimensional Hubbard model on the square lattice relevant to the cuprates. More accurate Quantum Monte Carlo simulations provide further ways to improve this approach[27, 28], and realistic electronic structures can be incorporated via the use of theories such as LDA+U[29] and LDA+DMFT[30] by utilizing the method of projectors.

Our own recent combination of the LDA with FLEX and RPA[31] (LDA+FLEX) has allowed us to extend these methodologies to incorporate  $\mathbf{k}$ - and  $\omega$  dependence of the electronic self-energy by evaluating dynamical spin and charge susceptibilities in a restricted Hilbert space

given by correlated orbitals. With a further extension of this method to compute the FLEX interaction vertices for the Cooper pairs[32], the description of unconventional superconductors in a realistic material framework became possible. Our most recent applications to  $\text{HgBa}_2\text{CuO}_4$ [32] recovered the known  $d_{x^2-y^2}$  symmetry of the order parameter here, and predicted various competing pairing states in a recently discovered superconducting nickelate  $\text{La}_3\text{Ni}_2\text{O}_7$  [33] and in vanadium kagome metal  $\text{CsV}_3\text{Sb}_5$ [34].

Estimates of the transition temperature  $T_c$  represent an additional challenge. In electron-phonon superconductors, it is typically calculated using Bardeen-Cooper-Schrieffer (BCS) theory[35] where the central quantity to determine is the coupling constant of the interaction  $\lambda$ , from which the  $T_c$  can be found via the McMillan equation[36]. Although this approach is straightforward, these estimates exhibiting exponential sensitivity to the errors in  $\lambda$  and uncertainties in the treatment of the Coulomb pseudopotential  $\mu^*$  usually serve to obtain the correct order of magnitude for the  $T_c$ . More rigorous Eliashberg theory of superconductivity requiring the input of the spectral function  $\alpha^2F(\omega)$  and the evaluation of the screened Coulomb interaction can be utilized to improve the accuracy of these estimates[37], but in a semi-quantitative way, the McMillan theory is known to suffice in many cases.

There are good reasons for the successes of the BCS approach, in particular, because in the electron-phonon superconductors the  $\alpha^2F(\omega)$  is limited by the Debye frequency  $\omega_D$  which is small comparing to the typical energies of the electronic states. For unconventional superconductors, technically, the Coulomb interaction vertex as, for example, given by FLEX, does not provide such a small parameter, therefore, many model calculations based on diagonalizing the BCS-type equations in case of spin fluctuations[25] necessitate additional assumptions. To overcome this difficulty, the Eliashberg equation can be solved directly on the imaginary Matsubara axis and predict the  $T_c$  directly[25, 38], but the methodology hides the transparency of the BCS approach which has allowed to guide the discoveries of many conventional superconductors by searching for the materials with large  $\lambda$ .

Here, we provide new insights to the superconductivity of single- and double-layer cuprates[39–46] by calculating their spin fluctuational spectral functions  $\alpha^2F(\omega)$  for a given pairing symmetry on the basis of frequency- and momentum-resolved FLEX-RPA pairing interaction and by utilizing their realistic LDA based electronic energy bands and wave functions. We first exactly diagonalize the linearized BCS gap equation and extract the highest eigenstate and the eigenvector as a function of the Fermi momentum set on a realistic Fermi surface of the material. We find the corresponding superconducting gap functions to be of  $d_{x^2-y^2}$  symmetry in all studied cuprates for a wide range of on-site Coulomb repulsions

$U$  and dopings that we scan during our simulations. We further utilize the Kramers-Kronig relations for the frequency dependence of the FLEX vertex, and its averaging over the eigenvectors provides a frequency resolution for each eigenstate. This gives rise to the definition of the spectral functions  $\alpha^2F(\omega)$  whose inverse frequency moments correspond to the eigenvalues of the BCS gap equation.

Our calculated material specific  $\alpha^2F(\omega)$  are found to exhibit remarkable similarities characterized by a sharp peak in the vicinity of 40–60 meV which has been known to exist from a wealth of experimental data in cuprates such, e.g., imaginary spin susceptibility accessible via the neutron scattering experiment[47], the existence of a 40 meV resonance visible in the superconducting state[48], as well as the kinks in the one-electron spectra seen at this energy range in angle resolved photoemission (ARPES) experiment[49]. We also find that  $\alpha^2F(\omega)$  decays rapidly at higher frequencies which justifies the use of the BCS-type treatment in the cuprates.

The maximum eigenvalue  $\lambda_{\text{max}}$  deduced from this procedure represents a spin fluctuational coupling constant similar to the electron-phonon (e-p)  $\lambda_{e-p}$ . We find it to be particularly large when the system is close to SDW, which in this theory appears for a particular value of  $U = U_{SDW}$ , that corresponds to the divergent static spin susceptibility at some wavevector. To allow evaluation of the  $T_c$  via the McMillan theory, we calculate the normal state self-energy and extract the electronic mass enhancement  $m^*/m_{LDA} = 1 + \lambda_{sf}$ . The mass enhancement is also large in the vicinity of SDW. However, the evaluated renormalized coupling constant  $\lambda_{eff} = \lambda_{\text{max}} / (1 + \lambda_{sf})$  that determines the BCS  $T_c$  was found to be modest unless we tune  $U$  to be within a few percent of  $U_{SDW}$ . Several numerical approaches to find  $U$  were proposed and applied to the cuprates in the past, such as constrained Random Phase Approximation (cRPA)[50, 51], or fitting  $U$  to reproduce some experiments, but such a great sensitivity to the proximity to  $U_{SDW}$  rules out the applicability of these methods here.

As the oldest and most extensively studied family of unconventional superconductors, cuprates provide a wealth of published mass enhancement data that can be extracted from ARPES, quantum oscillation and specific heat experiments. This data offer additional comparisons with the values of  $\lambda_{sf}$  that we calculate in the hope to find further constrains for the material specific  $U$  that is needed to predict the  $T_c$ . However, when comparing experimental data with theoretical predictions, different experimental techniques require specific considerations. For example, ARPES measures a two-dimensional spectral function, from which the Fermi velocity  $v_F^*$  can be extracted. Quantum oscillation studies use magnetic fields to induce oscillations around the Fermi surface. The frequency of these oscillations provides a measurement of the effective mass  $m^*$ . Specific heat measurements give

the electronic specific heat coefficient  $\gamma^*$  found from all bands. Many of these experiments are surveyed in our work but the spread in the deduced values of  $\lambda_{sf}$ , while being well within our theoretical predictions, does not offer further tuning of the constraints on the best determination of  $U$ .

The results presented here highlight challenges in building first-principle theories of high-temperature superconductivity but still offer new insights that go beyond previous treatments, such as the calculations of  $\alpha^2 F$ 's, the confirmation of the usability of approximate BCS-like  $T_c$  equations, and the evaluation of the material specific coupling constant  $\lambda$  without reliance on the tight-binding approximations of their electronic structures.

This paper is organized as follows. In Section II we survey our LDA+FLEX method and describe the numerical procedure to calculate the spin fluctuational spectral functions  $\alpha^2 F(\omega)$ . In Section III we report our results on the calculated behavior of superconducting energy gaps,  $\alpha^2 F(\omega)$ , the coupling constants  $\lambda_{\max}$  and the mass enhancement parameters  $\lambda_{sf}$  for a series of single- and double-layer high- $T_c$  cuprates. In Section IV we analyze available experimental data on the electronic mass renormalization deduced from ARPES[52–63], quantum oscillations[64–72] and measured values of the specific heat[73–76]. Section V is the conclusion.

## II. METHOD

The LDA+FLEX formalism describes a spin-dependent interaction between electrons[32, 33], with the common approximation that interactions occur near the Fermi surface. The interaction is denoted by

$$K^{\nu_1\nu_2\nu_3\nu_4}(\mathbf{r}_1, \mathbf{r}_2, \mathbf{r}_3, \mathbf{r}_4, \omega). \quad (1)$$

In the non-relativistic formalism, the spin space remains fully invariant. This vertex can be decomposed into charge  $K^c$  and spin  $K^s$  components based around the Pauli matrices

$$K^{\nu_1\nu_2\nu_3\nu_4} = \frac{1}{2}\delta_{\nu_1\nu_3}\delta_{\nu_2\nu_4}K^c - \frac{1}{2}\sigma_{\nu_1\nu_3}\sigma_{\nu_2\nu_4}K^s. \quad (2)$$

This decomposition facilitates a transformation into singlet-triplet space, where

$$K^{(S)} = \frac{1}{2}K^c - \frac{1}{2}E_s K^s \quad (3)$$

with  $E_{S=0} = -3, E_{S=1} = 1$ . Projecting the scattering from the Cooper pair wave functions  $\Psi_{\mathbf{k}j,SS_z}(\mathbf{r}_1, \mathbf{r}_2)$  onto  $K$  further reduces the vertex. Here  $\mathbf{k}$  is the momentum vector,  $j$  the band index,  $S$  and  $S_z$  are the spin and its  $z$ -projection for the Cooper pair. This results in the matrix  $M$ :

$$M_{\mathbf{k}j\mathbf{k}'j'}^{(S)}(\omega) = \langle \Psi_{\mathbf{k}j,SS_z} | K^{(S)}(\omega) | \Psi_{\mathbf{k}'j',SS_z} \rangle \quad (4)$$

Due to the Bloch-wave property of the Cooper pair wave functions, the lattice Fourier transforms with  $\mathbf{k}$  and  $\mathbf{k}'$  of the interaction

$$K_{\mathbf{k},\mathbf{k}'}^{(S)}(\mathbf{r}_1, \mathbf{r}_2, \mathbf{r}_3, \mathbf{r}_4, \omega) = \sum_{R_{1,2,3,4}} e^{-i\mathbf{k}(\mathbf{R}_1 - \mathbf{R}_2)} e^{i\mathbf{k}'(\mathbf{R}_3 - \mathbf{R}_4)} K^{(S)}(\mathbf{r}_1 - \mathbf{R}_1, \mathbf{r}_2 - \mathbf{R}_2, \mathbf{r}_3 - \mathbf{R}_3, \mathbf{r}_4 - \mathbf{R}_4, \omega), \quad (5)$$

are only relevant in the expression (4), where one lattice sum should be dropped out due to translational periodicity.

The Cooper pair wave functions are constructed from single-electron states, easily accessible in density functional theory (DFT). The formidable problem is the evaluation of the pairing interaction  $K^{(S)}$ . This vertex is approximated to operate for a correlated subset of electrons that are introduced with help of site dependent projector operators  $\phi_a(\mathbf{r}) = \phi_l(r) i^l Y_{lm}(\hat{r})$ . These operators originate from the one-electron Schrödinger equation taken with a spherically symmetric part of the full potential. The Hilbert space inside the correlated site reduces the full orbital set to a subset of correlated orbitals, such as the  $l = 2$  orbitals for Cu. Decomposing the  $K^{(S)}$  vertex in this manner yields the representation

$$K_{\mathbf{k},\mathbf{k}'}^{(S)}(\mathbf{r}_1, \mathbf{r}_2, \mathbf{r}_3, \mathbf{r}_4, \omega) = \sum_{a_1 a_2 a_3 a_4} K_{a_1 a_2 a_3 a_4}^{(S)}(\mathbf{k}, \mathbf{k}', \omega) \times \phi_{a_1}(\mathbf{r}_1) \phi_{a_2}(\mathbf{r}_2) \phi_{a_3}^*(\mathbf{r}_3) \phi_{a_4}^*(\mathbf{r}_4). \quad (6)$$

Evaluating this vertex with FLEX, using the on-site Coulomb interaction matrix  $I_{a_1 a_2 a_3 a_4}$  gives the final vertex equation:

$$\hat{K} = \hat{I} + \hat{I} \left( \hat{\chi} - \frac{1}{2} \hat{\pi} \right) \hat{I}, \quad (7)$$

where the interacting susceptibility  $\hat{\chi} = \hat{\pi} \left( \hat{1} - \hat{I} \hat{\pi} \right)^{-1}$  contains the non-interacting polarizability  $\hat{\pi}$ , and the subtraction of  $\frac{1}{2} \hat{\pi}$  removes the single bubble diagram that appears in both the bubble and ladder series. The  $\hat{I}$  matrix is built off the Hubbard term  $U$  and is local in space. This locality condition allows  $K_{a_1 a_2 a_3 a_4}^{(S)}(\mathbf{k}, \mathbf{k}', \omega)$  to be only dependent on  $\mathbf{k} \pm \mathbf{k}'$ . Taking the full interactions is computationally demanding, scaling as  $N_{atom}^4 N_{orb}^4$ . However, as previously reviewed[32], the local approximation reduces the complexity to scale with  $N_{atom}^2$ , and the use of only correlated orbitals minimizes the  $N_{orb}^4$  term, making the computations feasible.

The resulting matrix elements of the pairing interaction taken in Eq.(4) for  $\omega = 0$  are Hermitian and are used in the linearized BCS gap equation

$$\Delta_S(\mathbf{k}j) = - \sum_{\mathbf{k}'j'} M_{\mathbf{k}j\mathbf{k}'j',Re}^{(S)}(0) \frac{\tanh(\epsilon_{\mathbf{k}'j'}/2T_c)}{2\epsilon_{\mathbf{k}'j'}} \Delta_S(\mathbf{k}'j'). \quad (8)$$

Here  $\epsilon_{\mathbf{k}j}$  denotes the non-interacting band structure from which the superconducting state evolves, and  $T_c$  is the critical temperature, below which superconductivity exists. We focus only on interactions occurring near the Fermi surface, taking the BCS approximation that all other interactions beyond  $\omega_c$  are zero. As a standard practice, we also multiply the left part of this equation with a parameter  $\varepsilon$  playing the role of the eigenvalue, and treat  $\Delta_S(\mathbf{k}j)$  as the eigenvector. This results in

$$-\ln\left(\frac{1.134\omega_c}{T_c}\right) \sum_{j'} \int_{FS} \frac{dS_{\mathbf{k}'}}{|v_{\mathbf{k}'j'}|} M_{\mathbf{k}j\mathbf{k}'j',Re}^{(S)}(0) \Delta_S(\mathbf{k}'j') = \varepsilon \Delta_S(\mathbf{k}j), \quad (9)$$

where the integration is extended over the Fermi surface only. To view this expression as diagonalization in  $\mathbf{k}j\mathbf{k}'j'$  indexes, we introduce the renormalized eigenvalues  $\lambda = \varepsilon / \ln\left(\frac{1.134\omega_c}{T_c}\right)$ , and, since the physical solution for  $\Delta_S(\mathbf{k}j)$  is given when the highest eigenvalue  $\varepsilon$  becomes unity, the highest renormalized eigenvalue  $\lambda_{\max}$  is the coupling constant that produces the famous BCS equation for  $T_c = 1.134\omega_c \exp(-1/\lambda_{\max})$ .

McMillan's  $T_c$  equation uses this coupling constant to determine  $T_c$ , but unlike the BCS, it also takes renormalization and higher-energy damping terms into account. The coupling constant  $\lambda_{\max}$ , the mass enhancement factor  $\lambda_{sf}+1$  and the higher energy Coulomb repulsion term  $\mu_m^*$  make up the 3 parameters in the effective coupling constant used in the  $T_c$  equation, analogous to McMillan's:

$$T_c \approx \omega_c \exp(-1/\lambda_{eff}) \quad (10)$$

$$\lambda_{eff} = \frac{\lambda_{\max} - \mu_m^*}{\lambda_{sf} + 1} \quad (11)$$

The cutoff frequency  $\omega_c$  is often taken to be the resonant peak seen in neutron scattering experiments[77, 78], found to be about 40meV. Similar energy scales are seen in photoemission experiments as a kink in the emission spectrum[49]. The renormalization constant  $\lambda_{sf}$  can be derived from the normal state self-energy at the Fermi surface:

$$\lambda_{sf} = -\left\langle \frac{\partial \Sigma(\mathbf{k}, \omega)}{\partial \omega} \Big|_{\omega=0} \right\rangle_{FS}. \quad (12)$$

The parameter  $\mu_m^*$  is usually small in standard  $s$ -wave superconductors ( $\sim 0.1$ ) but here it refers to the same pairing symmetry as the eigenvalue  $\lambda_{\max}$ . We expect it to be

negligible for the  $d$ -wave symmetry as the projection of the screened Hubbard interaction onto  $d_{x^2-y^2}$  cubic harmonic is known to be very small [79].

Finally, we describe the calculation of the Eliashberg spectral function  $\alpha^2 F(\omega)$ . Since the real and imaginary parts of the interaction (1) obey the Kramers-Kronig relation, we can relate the matrix elements (4) that appear for  $\omega = 0$  in the solution of the BCS equation (9) to the matrix elements taken over the imaginary part of the interaction (1):

$$M_{\mathbf{k}j\mathbf{k}'j',Re}^{(S)}(0) = \frac{2}{\pi} \int_0^\infty \frac{M_{\mathbf{k}j\mathbf{k}'j',Im}^{(S)}(\omega) d\omega}{\omega}. \quad (13)$$

Let us represent the eigenvalues of (9) as the averages over the eigenvectors

$$\lambda_{\max} \equiv \lambda_{Re}(0) = \sum_{jj'} \int \int_{FS} \frac{dS_{\mathbf{k}}}{|v_{\mathbf{k}j}|} \frac{dS_{\mathbf{k}'}}{|v_{\mathbf{k}'j'}|} \times \Delta_S^*(\mathbf{k}j) M_{\mathbf{k}j\mathbf{k}'j',Re}^{(S)}(0) \Delta_S(\mathbf{k}'j'). \quad (14)$$

We arrive to the spectral resolution for the eigenvalues

$$\lambda_{Re}(0) = \frac{2}{\pi} \int_{0+}^\infty \frac{\lambda_{Im}(\omega) d\omega}{\omega}, \quad (15)$$

$$\lambda_{Im}(\omega) = \sum_{jj'} \int \int_{FS} \frac{dS_{\mathbf{k}}}{|v_{\mathbf{k}j}|} \frac{dS_{\mathbf{k}'}}{|v_{\mathbf{k}'j'}|} \times \Delta_S^*(\mathbf{k}j) M_{\mathbf{k}j\mathbf{k}'j',Im}^{(S)}(\omega) \Delta_S(\mathbf{k}'j'). \quad (16)$$

Thus,  $\lambda_{Im}(\omega)$  is related to the Eliashberg spectral function for every eigenstate of the BCS equation as follows:

$$\alpha^2 F(\omega) = \frac{1}{\pi} \lambda_{Im}(\omega). \quad (17)$$

### III. RESULTS

The method described above allows for the complete calculation of material specific superconducting energy gaps,  $\alpha^2 F(\omega)$  and coupling constants without the need for band structure approximations. It allows us to resolve the gap functions and the corresponding pairing symmetries for realistic Fermi surfaces which is a step beyond previous tight-binding calculations.

We use the full potential linear muffin-tin orbital method [80] to calculate LDA energy bands and wave functions for a series of single- and double layer cuprates. We then utilize the LDA+FLEX(RPA) evaluation of the pairing interaction  $K_{a_1 a_2 a_3 a_4}^{(S)}(\mathbf{q}, \omega)$  on three dimensional grids of the  $\mathbf{q}$  points in the Brillouin Zone. The Fermi surface is triangularized onto small areas described by several thousands of Fermi momenta for which the matrix

elements of scattering between the Cooper pairs, Eq.(4), are evaluated. The linearized BCS gap equation (9) is then exactly diagonalized and the set of eigenstates is obtained for both  $S = 0$  and  $S = 1$  pairings. The highest eigenvalue  $\lambda_{\max}$  represents the physical solution and its eigenvector corresponds to the superconducting gap  $\Delta_S(\mathbf{k}j)$ .

We use Hubbard interaction parameter  $U$  for the  $d$ -electrons of Cu as the input to this simulation. We first vary  $U$  to determine the divergency of the static spin susceptibility which usually occurs at or very close to the antiferromagnetic ordering wavevector  $\mathbf{q}_{AF} = (\pi, \pi, 0)$ . This sets the upper bound,  $U_{SDW}$ , whose value for each cuprate is listed in Table 1. We can subsequently vary  $U$  for the range of values less than  $U_{SDW}$ .

We also introduce the doping by holes using the virtual crystal approximation. A whole range of dopings  $\delta \leq 0.5$  (we refer  $\delta$  per single  $\text{CuO}_2$  plane) is studied in our work but, since within RPA the SDW instability always exist for some  $U_{SDW}$  at any doping, the doping dependence of the results cannot be traced in our method. We therefore present most of our results for the doping level equal to 0.1 hole per  $\text{CuO}_2$  plane unless otherwise noted.

### a. Pairing Symmetries

The result of our simulation for superconducting energy gaps is shown on Fig. 1 where the calculated  $\Delta_{S=0}(\mathbf{k}j)$  exhibit a much celebrated  $d_{x^2-y^2}$ -symmetry for 8 cuprates that are studied in this work. The blue/red color corresponds to negative/positive values of  $\Delta$ . The zeroes of the gap function are along (11) direction which are colored in grey. Fig. 1 utilizes the doping level equal to 0.1 hole per  $\text{CuO}_2$  plane, although the result is robust for the range of dopings  $\delta \leq 0.3$  and also for the range of  $U; U_{SDW}$  that we used in the simulation. The effect of higher dopings  $\delta = 0.4 - 0.5$  has been checked, but at those levels the gap function was found to develop a rather complex sign-changing behavior along the lobes by acquiring higher order harmonics. Such solutions would carry an additional kinetic energy and should be less favorable energetically.

We now turn to the material dependence of our results.  $\text{HgBa}_2\text{CuO}_4$  is one of the simplest single-layer cuprates, with large spacer layers separating the  $\text{CuO}_2$  superconducting planes. As a result, its Fermi surface is made of just four hole pockets forming a kind of rounded cross shape. This fundamental shape is present in all of the cuprates, though the Fermi surface of  $\text{La}_2\text{CuO}_4$  is much more diamond-like. Omitting the complications introduced by multiple bands, such as those in  $\text{YBa}_2\text{Cu}_3\text{O}_7$ , the addition of holes gradually transforms the Fermi surface of each cuprate to resemble that of  $\text{La}_2\text{CuO}_4$ , reducing the electron-filled area within the Brillouin zone. This also alters the dominant wavevector  $\mathbf{q}$  that leads to

the maximum Fermi surface nesting.

$\text{YBa}_2\text{Cu}_3\text{O}_7$  is a particularly interesting material. The  $\text{CuO}_2$  planes, as well as the  $\text{CuO}$  chains that occur underneath, lead to a complicated Fermi surface. There are a number of pockets appearing from the many band crossings that result from the  $\text{Cu-O}$  planes and chains, not all of them superconducting. While red and blue represent positive and negative signs for the superconducting gap function, gray represents values closer to zero. In materials where the entirety of the Fermi surface contributes to the interaction, the gray points represent nodes where the gap vanishes. This can be seen in all of the superconducting plots in Fig. 1, where the red section meets the blue section.

The  $d_{x^2-y^2}$  Cu orbitals are known to be correlated and lead to superconductivity, but this is not true of all orbitals, even those at the Fermi surface. In those cuprates where uncorrelated states are present at the Fermi level, the associated bands fail to develop a superconducting gap. In particular, materials such as  $\text{YBa}_2\text{Cu}_3\text{O}_7$ ,  $\text{Tl}_2\text{Ba}_2\text{CuO}_6$ , and  $\text{Tl}_2\text{Ba}_2\text{CaCu}_2\text{O}_8$  display those states, which can be seen in the gray pockets in the corners of the Brillouin Zone. Another key feature is the region of the Fermi surface around the  $\Gamma$  point, where the gap function approaches zero, a characteristic absent in other cuprates. Each of the Thallium compounds contain an electron pocket around the  $\Gamma$  point that does not contribute to superconductivity.

$\text{La}_2\text{CuO}_4$  and  $\text{Bi}_2\text{Sr}_2\text{CaCu}_2\text{O}_8$  each exhibit Fermi surfaces that are more diamond-shaped than the other cuprates, though  $\text{La}_2\text{CuO}_4$  has a much simpler Fermi surface. As doping increases for these materials, the Fermi surface shrinks in a different manner than the other cuprates. This can lead to a possible unusual behavior. While this is an active area of research, recent studies show that significantly overdoped materials of this nature are still superconducting[61].

Experimental work is scarce for  $\text{Sr}_2\text{CuO}_2\text{Cl}_2$  and  $\text{CaCuO}_2$ . The latter is the simplest infinite layer cuprate but likely metastable. Notably the structure of  $\text{HgBa}_2\text{CuO}_4$  and  $\text{CaCuO}_2$  are extremely similar as both are tetragonal. Though  $\text{CaCuO}_2$  seems physically not realized in its bulk form, both materials are expected to give high critical temperatures.  $\text{Sr}_2\text{CuO}_2\text{Cl}_2$  has a similar Fermi surface as  $\text{HgBa}_2\text{CuO}_4$ , though the gap function is much sharper as the nodes can be seen as taking up less space in Fig. 1. A gap function with smoother nodes has a smaller kinetic energy and so is more energetically favorable.

### b. $\alpha^2 F(\omega)$ Spectral Functions

The Eliashberg spectral functions that we calculate using our LDA+FLEX(RPA) method are displayed in Fig. 2, where  $\alpha_{x^2-y^2}^2 F(\omega)$  represents frequency reso-

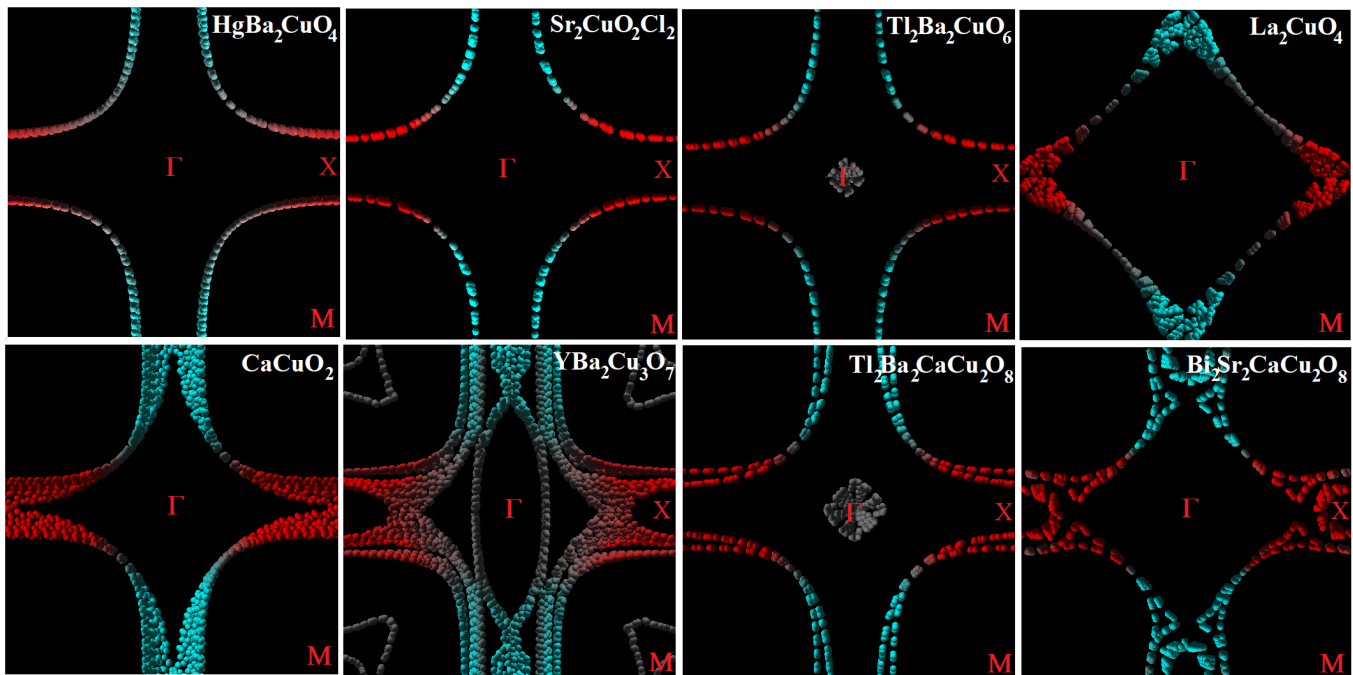


FIG. 1: Superconducting energy gap functions  $\Delta(\mathbf{k})$  for 8 cuprates as a function of the Fermi surface wave vector (top view of the 3 dimensional Fermi surface is shown) calculated using numerical solution of the linearized BCS gap equation with the singlet pairing interaction evaluated via the LDA+FLEX(RPA) approach. The  $d_{x^2-y^2}$  pairing symmetry is seen in all cases as a sliding color scale with red corresponding to a large positive gap, blue a large negative gap, and gray the zero gap. The doping level is set to 0.1 holes per  $\text{CuO}_2$  layer.

lution of the highest eigenvalue  $\lambda_{\max}$  corresponding to the  $d_{x^2-y^2}$  symmetry, and  $\alpha_{sf}^2 F(\omega)$  gives frequency resolution of the mass enhancement parameter  $\lambda_{sf}$ . These functions are material-dependent, have different height, width and shape, and the eigenvalue resolution they display is unique to each material. However, they also exhibit several universal features such as the existence of a sharp peak at low frequencies, followed by a drop-off, which is most pronounced for  $\alpha_{x^2-y^2}^2 F(\omega)$ . This drop-off points to a separation of the energy scales, and justifies the use of McMillan-like  $T_c$  equation that relies on the existence of a cutoff frequency for the pairing interaction.

The  $d$ -wave superconducting spectral functions shown by the red lines in Fig. 2 possess low-frequency peaks most clearly. The spectral functions  $\alpha_{sf}^2 F(\omega)$ , displayed in blue do not always show this behavior despite both  $\alpha_{sf}^2 F(\omega)$  and  $\alpha_{x^2-y^2}^2 F(\omega)$  originate from the same interaction vertex (1), and they are generally expected to exhibit similar shapes. Some materials have  $\alpha_{sf}^2 F(\omega)$  that somewhat mimic the falloff in the  $d$ -wave projection, which for instance, seen in  $\text{HgBa}_2\text{CuO}_4$  and  $\text{CaCuO}_2$ . Other materials have additional peaks, beyond the first at low frequency, whose shape does not necessarily match those of its  $d$ -wave counterpart.

For all materials, the precise location of the low-frequency peak changes as a function of  $U$ . As  $U$  gets closer to  $U_{SDW}$ , the peaks shift to lower frequencies un-

til they diverge at  $\omega = 0$  when  $U = U_{SDW}$ . The precise values of  $U$  that are used to generate the spectral functions in Fig. 2 are listed in Table 1, column  $U_{SC}$ . We select these  $U$ 's to roughly reproduce the experimental values of  $T_c$ , the procedure to be described in details in the next section. Here we note that such a choice generates the low-frequency peaks in  $\alpha_{x^2-y^2}^2 F(\omega)$  in the region of 40–60 meV. Experimental methods such as neutron scattering[78] and ARPES[52] have indicated, respectively, that there are peaks and kinks found at similar energies for cuprates. Although the detailed comparison of these values is immature, the agreement between theory and experiment in the approximate energy scale is a good sign of the internal consistency in our selected values of  $U$ .

The effective coupling constant in Eq.(11) is determined by the ratio of  $\lambda_{\max}$  to  $\lambda_{sf} + 1$ . Both  $\lambda_{\max}$  and  $\lambda_{sf}$  being the integrals over the spectral function divided by  $\omega$ , are sensitive to the low-frequency part of the spectrum, that in turn is most sensitive to  $U$ . Altering  $U$  shifts the location of each peak, and if these peaks shift together with one function roughly following the other, then the effective coupling constant  $\lambda_{eff}$  evolves smoothly with  $U$  and does not diverge.

We find that cuprates follow this pattern unless  $U$  gets very close to its SDW instability point,  $U_{SDW}$ . Fig.3 shows our calculated dependence of the maximum eigen-

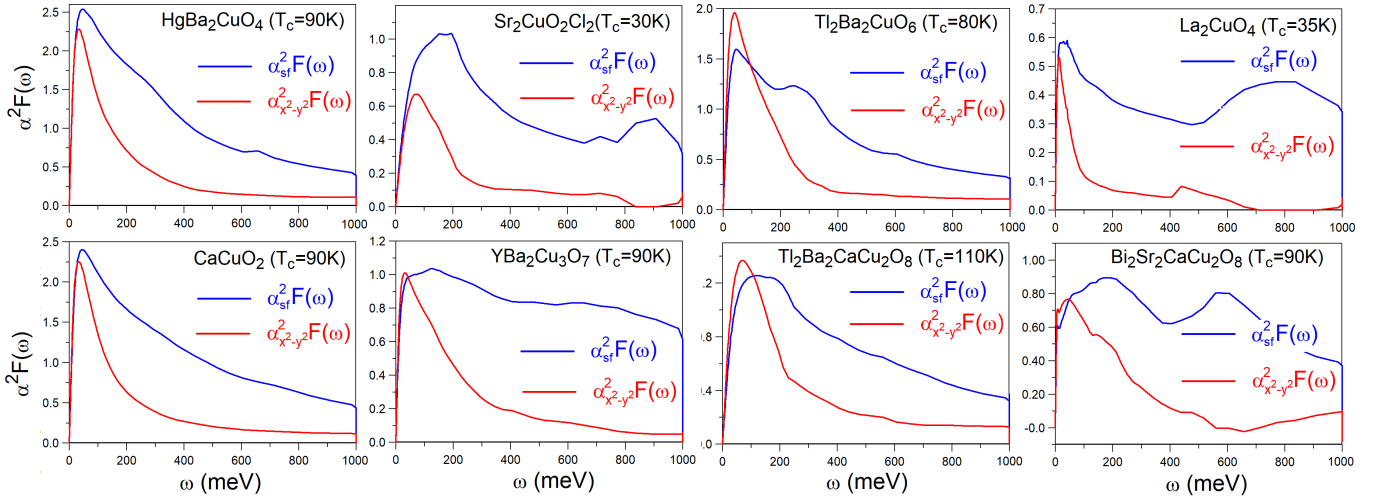


FIG. 2: Eliashberg spectral functions for 8 different cuprates calculated using the LDA+FLEX(RPA) method. Spectral function  $\alpha_{x^2-y^2}^2 F(\omega)$  (red lines) represents frequency resolution of the highest eigenvalue  $\lambda_{\max}$  of the BCS gap equation corresponding to the  $d_{x^2-y^2}$  symmetry, and  $\alpha_{sf}^2 F(\omega)$  (blue lines) gives frequency resolution of the mass enhancement parameter  $\lambda_{sf}$ .

value  $\lambda_{\max}$  corresponding to the  $d_{x^2-y^2}$  symmetry and the spin fluctuational mass enhancement parameter  $\lambda_{sf}$ , as a function of  $U$  for the hole doping  $\delta = 0.1$  per  $\text{CuO}_2$  plane. The effective coupling constant  $\lambda_{eff} = \lambda_{\max}/(1 + \lambda_{sf})$  is shown on the right scale. One can see that the range of values of  $\lambda_{eff}$  is quite modest for a wide interval of  $U$ 's as compared to both  $\lambda_{\max}$  and  $\lambda_{sf}$ , primarily due to the fact that the rise in the eigenvalue of the gap equation, is compensated by the renormalization effect of the electronic self-energy. This is, in particular, the case for  $\text{HgBa}_2\text{CuO}_4$  and  $\text{CaCuO}_2$ , each of which have roughly  $1\text{eV}$  of leeway in the value of  $U$ . Interestingly,  $\text{YBa}_2\text{Cu}_3\text{O}_7$  shows similar behavior: with a very flat  $\alpha_{sf}^2 F(\omega)$ , its coupling constants also keeping pace with each other well as  $U$  increases.

Other cuprates have smaller ranges of allowable  $U$  interaction strengths but their  $\alpha^2 F$ 's behave in a similar manner.  $\text{YBa}_2\text{Cu}_3\text{O}_7$ ,  $\text{Bi}_2\text{Sr}_2\text{CaCu}_2\text{O}_8$  and both Thallium-based compounds have sharper peaks in  $\alpha_{x^2-y^2}^2 F(\omega)$  than their  $\alpha_{sf}^2 F(\omega)$  counterparts. The divergence and shift towards the origin as  $U$  increases affects the respective coupling constants. As the Hubbard term approaches  $U_{SDW}$ , the  $\lambda_{\max}$  eigenvalue that results from  $\alpha_{x^2-y^2}^2 F(\omega)$  increases faster than the mass renormalization  $\lambda_{sf} + 1$ , because the low frequency peak is much sharper for  $\alpha_{x^2-y^2}^2 F(\omega)$  and starts to diverge first. This is seen both in Fig.2 and also in Fig. 3 at the  $U$  point where  $\lambda_{\max}$  meets  $\lambda_{sf}$ . The impact is seen in how quickly  $\lambda_{eff}$  increases in this region. While this effect is not very large for most materials, it provides a window of opportunity to find the elevated values of  $\lambda_{eff}$  needed to explain the high  $T_c$ 's.

At high energies, though not displayed in Fig. 2, our calculated  $\alpha^2 F$ 's raise rapidly as plasmons begin to pos-

sess some spectral weight, a factor that is normally taken into the  $\mu^*$  calculations of McMillan's equation.

### c. Coupling Constants and the $T_c$

Near the SDW instability, the choice of the Hubbard term  $U$  has a significant impact on the coupling constant and the resulting critical temperature  $T_c$ . However, methods such as cRPA are not guaranteed to deliver the precise determination of  $U$  as they tend to have much larger inaccuracies [50, 51]. This prompts us to consider more empirical pathways.

Our calculations of  $\lambda_{\max}$ ,  $\lambda_{sf}$  and  $\lambda_{eff}$  as a function of  $U$  presented in Fig. 3 allow us to perform comparisons between theory and experiment. For example, mapping measured mass enhancement data onto the FLEX-based  $\lambda_{sf}$  can determine the corresponding  $U$  for which the experiment can be reproduced, and further  $\lambda_{eff}$  to see whether one can obtain a reasonable estimate of  $T_c$ . In Table 1, we give the compilation of the experimentally extracted  $\lambda_{sf}$  where the third, fourth, and fifth columns indicate the values of  $\lambda_{sf}$  found from ARPES, quantum oscillations and the specific heat data (figures in brackets indicate the doping at which the measurement was taken). Although we provide a complete survey of the experimental results in the next section, here we note the existence of a rather large spread in the experimentally deduced  $\lambda_{sf}$  which prevents us from concluding on what is the 'right'  $U$  to be used by the theory.

One can take the experimentally known  $T_c$  and determine such  $\lambda_{eff}$  for which it can be reproduced from Eq.(10). This however needs an input of the cutoff frequency  $\omega_c$ . Experimentally, in cuprates the spin fluctuational frequencies have been seen in the proximity to 40

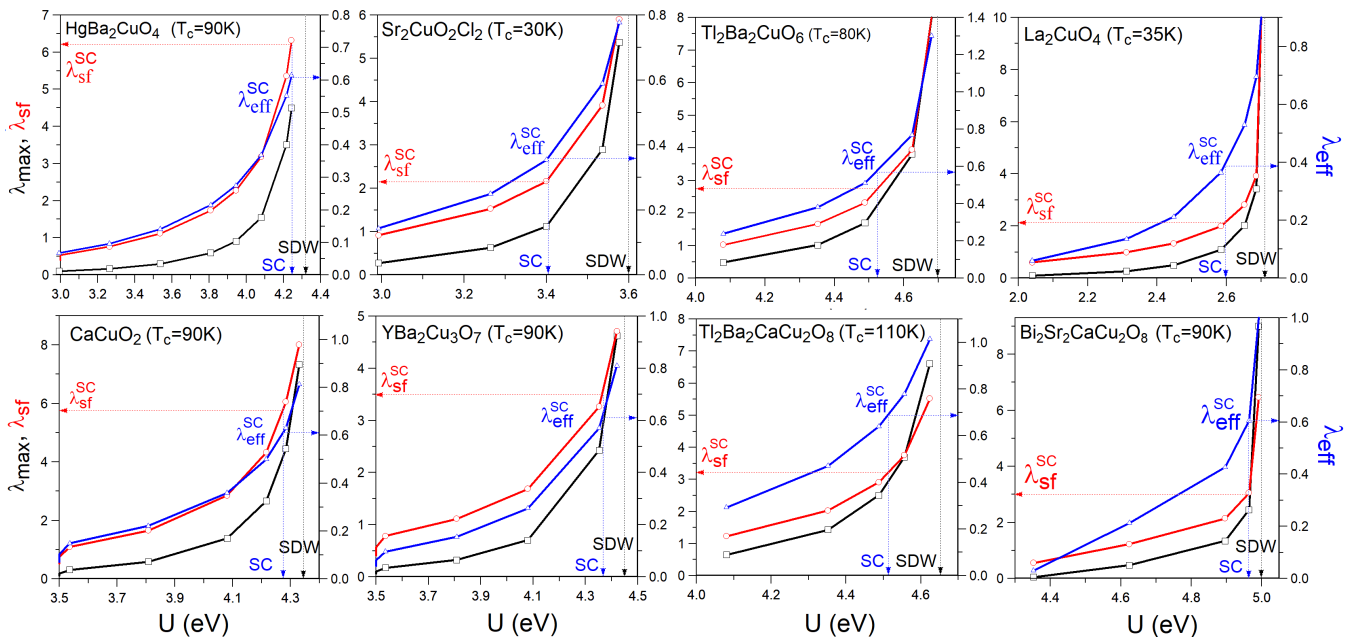


FIG. 3: Calculated using LDA+FLEX(RPA) method dependence of the maximum eigenvalue  $\lambda_{\max}$  corresponding to the  $d_{x^2-y^2}$  symmetry and the spin fluctuational mass enhancement parameter  $\lambda_{sf}$ , as a function of the on-site Hubbard interaction  $U$  for d-electrons of Cu in a series of cuprate superconductors for the hole doping  $\delta = 0.1$  per  $\text{CuO}_2$  plane. The effective coupling constant  $\lambda_{eff} = \lambda_{\max}/(1 + \lambda_{sf})$  is shown on the right scale. Sample values are selected with dotted lines showing how to extrapolate the coupling constants from these plots:  $\lambda_{eff}^{SC}$  is selected on the right  $y$ -axis, giving a value of  $U_{SC}$  on the  $x$ -axis, from where the value of  $\lambda_{sf}^{SC}$  can be determined. Given the nature of the FLEX interaction terms, the coupling constants diverge in all of these graphs when  $U$  approaches the SDW instability point,  $U_{SDW}$ .

meV as peaks in imaginary spin susceptibility accessible via the numerous neutron scattering experiments[47]. A famous 40 meV resonance has been detected in the superconducting state[48]. Numerous ARPES experiments showed kinks in the one-electron spectra at the same energy range[49]. These kinks are sometimes interpreted as due to the electron-phonon interactions[81], but, unfortunately, the calculated values of  $\lambda_{e-p}$  are known to be small in the cuprates[82, 83].

Taking  $\omega_c = 40$  meV, and the experimental  $T_c$  (shown for each cuprate in the second column of Table 1), we have determined the values of  $\lambda_{eff}$  by inverting Eq.(10). These values are indicated in Fig. 3 by labeling  $\lambda_{eff}$  with abbreviation 'SC' (superconducting). One can subsequently use this data in Fig. 3 to find the corresponding values of  $U$  and  $\lambda_{sf}$ . We indicate the obtained  $U$  by arrow 'SC' on the horizontal axis of Fig.3 and the obtained mass enhancement parameter by  $\lambda_{sf}^{SC}$ . We also indicate by arrow on horizontal axis of Fig. 3 the obtained values of  $U_{SDW}$  that correspond to the SDW divergence. All data deduced from this procedure,  $\lambda_{eff}^{SC}$ ,  $\lambda_{sf}^{SC}$ ,  $\lambda_{\max}^{SC}$ ,  $U_{SC}$  are also listed in corresponding columns of Table 1.

One can see that in order to match experimental critical temperatures,  $U_{SC}$  needs to be very close to  $U_{SDW}$ . In every cuprate displayed,  $U_{SC}$  is less than 0.2 eV away from  $U_{SDW}$ . Different materials diverge faster or slower than others, giving less or more range of allowable  $U$  val-

ues.  $\text{HgBa}_2\text{CuO}_4$  and  $\text{YBa}_2\text{Cu}_3\text{O}_7$  both have this wide range. The materials with steeper dependence of  $\lambda$  vs.  $U$  have much more restricted values of  $U$ , particularly  $\text{Bi}_2\text{Sr}_2\text{CaCu}_2\text{O}_8$ , for which the allowed value of  $U$  can be found with much higher accuracy.

By using the same  $\omega_c = 40$  meV [84], comparisons of materials with similar critical temperatures can be made.  $\text{HgBa}_2\text{CuO}_4$ ,  $\text{CaCuO}_2$ ,  $\text{YBa}_2\text{Cu}_3\text{O}_7$ , and  $\text{Bi}_2\text{Sr}_2\text{CaCu}_2\text{O}_8$ , all have an effective  $\lambda$  just above 0.6. The relatively low choice of  $\omega_c$  pushes their  $U_{SC}$  values very close to  $U_{SDW}$  in order to reach the desired transition temperature.

One can also compare the estimated  $\lambda_{sf}^{SC}$  deduced from this procedure with their measured values.  $\text{HgBa}_2\text{CuO}_4$  requires  $\lambda_{sf}^{SC} = 6.2$ , which looks above the highest reported measurement, and so falls out of experimental bounds. Similar cases are seen for other superconductors, where  $\lambda_{sf}$  is seen to be typically overestimated by this theory although the spread in the experimental values is also large. It seems likely that the universal choice of  $\omega_c = 40$  meV is not the best option in trying to find a good match between theory and experiment.

We finally note that as hole doping increases, the Fermi surface shrinks as electrons are removed from the system, causing the nesting vector to become smaller. Thus, within our RPA treatment, the gap function gradually begins to incorporate a  $g$ -wave solution. This result con-



tradicts with a well-established experimental result that cuprates exhibit  $d$ -wave superconductivity at all dopings, with  $T_c$  showing a superconducting dome and decreasing on the overdoped side of the phase diagram. Several recent studies beyond RPA find the  $d$ -wave solution[26, 85], which reasonably mimics the shape of the superconducting dome. The presented approach can recover this behavior only if one allows the dependency of the Hubbard  $U$  vs. doping.

Though cRPA values are imprecise, several publications did indeed find that  $U$  decreases slightly with doping. A recent work[50] reported computation of doping dependent  $U$  using the constrained RPA procedure. Their reported values of  $U \approx 4$  eV for HgBa<sub>2</sub>CuO<sub>4</sub> are very close to the ones needed to produce large  $\lambda_{\text{max}}$ , as seen in our Fig. 3, together with the trend that  $U$  decreases with doping a little bit. In a different work employing dynamical cluster approximation (DCA) [86], an effective temperature dependent coupling  $\bar{U}(T)$  was introduced to parametrize the DCA pairing interaction in terms of the spin susceptibility. It was extracted between 2 and 4 eV and was shown to exhibit some reduction upon doping.

#### IV. ANALYSIS OF EXPERIMENT

Numerous studies have been conducted in the past to determine the electronic mass enhancement parameter  $\lambda_{sf}$  in cuprates. Usually, it can be found from one of three types of experiment: angle resolved photoemission, quantum oscillation, and specific heat measurements. We focus on seven cuprates and have extracted the values of  $\lambda_{sf}$  from the published data, displayed in Table 1. This data is compared with theoretical results found from the LDA+FLEX method.

There is considerable experimental uncertainty in both the value of  $\lambda_{sf}$  and its position on the doping axis of the phase diagram. Doping levels are often mapped based on  $T_c$ , which introduces imprecision in nominal doping[52]. Experiments are also quite sensitive to disorder induced scattering which can lead to additional inaccuracies in  $\lambda_{sf}$ .

There is a variation in experimental conditions that may affect this data as well. Specific heat measurements take into account all bands, not just those that contribute to superconductivity, and so can mislead our comparisons with the values of electronic mass renormalization that we calculate for correlated electrons only. Quantum oscillation experiments employ very high magnetic fields. The specific heat data taken at temperatures below  $T_c$  sometimes also employ magnetic fields to suppress superconducting phase. These conditions may alter the measured renormalization constants. APRES is generally a well-regarded method to determine normal-state electronic structure, but there can still be issues extrap-

olating  $\lambda_{sf}$  since it is a surface sensitive technique.

In Table 1, the renormalization parameters  $\lambda_{sf}$  extracted from experiment are taken either by direct quote from the publication, or approximately deduced from the paper's figures. Though straightforward, the method of extraction depends on the type of experiment and is discussed below.

##### a. Angle Resolved Photoemission

ARPES measures the energy band dispersions as a function of a two dimensional wavevector and neglects the  $k_z$  dispersion, but for cuprates with their quasi-2D crystal structures this is usually not a problem. Only some studies[87] note the non-zero  $c$ -axis conductivity, which, may be an issue for multilayered cuprates. Finite resolution makes band measurements inexact, and carry possibilities of missing some of the electronic spectral weight. Other studies note that ARPES shows significantly more scattering than Angular Magnetoresistance Oscillation (AMRO) experiments[54], and another study[88] claims that there is a nonzero density of states in the antiferromagnetic region that is too small for ARPES to spot.

Extracting data for  $\lambda_{sf}^{ARPES}$  that we show in Table 1 means finding the ratio of effective mass to the calculated band mass,  $m^*/m_{LDA}$ . This is done through the relation  $m^* = \hbar k_F/v_F^*$ , where by determining the Fermi momentum and the Fermi velocity the effective mass is found. Many ARPES studies show energy vs. momentum plots at different points along the Fermi surface. In this paper, the  $v_F^*$  value is taken at the point at or near the gap node as this is closest to the Fermi surface. Determining  $k_F$  at this point was done by finding the distance from  $\Gamma$  to the gap node in the plotted Fermi surface. Experimental values for the unit cell dimensions are taken for each material in order to find  $k_F$ . The energy vs. momentum curves often have significant width, the peak of which is found by mapping the functions onto a Lorentzian. These peaks are then tracked in order to find  $v_F^*$ . Determining the Lorentzian is not practical without the original data, and so we visually approximate the peak locations used in the determination of  $v_F^*$ . Finally after  $v_F^*$  and  $k_F$  are determined, they are used to calculate  $m^*$ .

##### b. Quantum Oscillations

The de Haas-van Alphen (dHvA) effect relies on the electrons oscillating around the Fermi surface to find values of their effective mass,  $m^*$ . Unfortunately, often scattering prevents quasiparticles from completing their orbit, which can throw off measured values. Additionally, one might expect similar results to be found across different experimental techniques, but AMRO may detect

TABLE I: Compilation of experimental and theoretical results for the high-temperature superconducting cuprates studied in this work. For each material, listed are its  $T_c(K)$  and mass enhancement parameter deduced from ARPES,  $\lambda_{sf}^{ARPES}$ , quantum oscillation,  $\lambda_{sf}^{dHvA}$ , and specific heat,  $\lambda_{sf}^{sp.heat}$  experiments. The values in brackets indicate the doping level (number of holes per one CuO<sub>2</sub> plane) for which the measurement was taken. Also listed are the values of Hubbard  $U_{SDW}$  (eV) that correspond to the SDW instability point seen via divergency of the static susceptibility, and the values of  $U_{SC}$  (eV) that are empirically determined from Fig.3 to reproduce the experimental  $T_c$  via the BCS  $T_c$  equation with  $\omega_c = 40meV$ . The theoretical coupling constants  $\lambda_{eff}^{SC}$ ,  $\lambda_{sf}^{SC}$ ,  $\lambda_{max}^{SC}$  that correspond to  $U_{SC}$  are also given.

Compound	$T_c^{exp}(K)$	$\lambda_{sf}^{ARPES}[\delta]$	$\lambda_{sf}^{dHvA}[\delta]$	$\lambda_{sf}^{sp.heat}[\delta]$	$\lambda_{eff}^{SC}$	$\lambda_{sf}^{SC}$	$\lambda_{max}^{SC}$	$U_{SC}(eV)$	$U_{SDW}(eV)$
HgBa <sub>2</sub> CuO <sub>4</sub>	90[39]	0.97[0.13][52]	3.11[0.096][64] 2.09[0.1][64] 1.59[0.101][64] 1.39[0.115][64] 2.08[0.133][64] 2.42[0.137][64] 3.68[0.152][64] 1.62[0.09][65] 1.89[0.09][66]	5.42[0.09][73, 74]	0.61	6.20	4.39	4.24	4.32
Sr <sub>2</sub> CuO <sub>2</sub> Cl <sub>2</sub>	30[40]	1.5[0.0][53]	—	—	0.36	2.22	1.16	3.40	3.60
Tl <sub>2</sub> Ba <sub>2</sub> CuO <sub>6</sub>	80[41]	~ 4[0.26][54]	1.88[0.297][67] 1.94[.270][67] 2.4[0.304][67] 2.42[0.3][68]	1.59[0.33][73, 74]	0.57	2.75	2.14	4.53	4.70
La <sub>2</sub> CuO <sub>4</sub>	35[42]	2.15[0.095][55] 2.85[0.125][55] 1.0[0.30][56] 1.1[0.15][56] 2.87[0.063][57]	1.53[0.16].[69]	0.5[0.33][73, 75] 2.4[0.22][76] 0.6[0.14][76] 2.08[0.24][76] 2.3[0.25][76]	0.39	2.10	1.21	2.60	2.71
CaCuO <sub>2</sub>	90[43]	—	—	—	0.61	5.57	4.01	4.27	4.34
YBa <sub>2</sub> Cu <sub>3</sub> O <sub>7</sub>	90[44]	1.27[0.073][58] 1.05[0.095][58] 1.03[0.18][58] 3.1[0.14 – 0.18][59]	0.45[0.1][70] 0.57[0.1][71] 0.24[0.109][72]	—	0.61	3.50	2.74	4.36	4.45
Tl <sub>2</sub> Ba <sub>2</sub> CaCu <sub>2</sub> O <sub>8</sub>	120[45]	1.8[0.16][60]	—	—	0.69	3.20	2.90	4.52	4.66
Bi <sub>2</sub> Sr <sub>2</sub> CaCu <sub>2</sub> O <sub>8</sub>	90[46]	0.3[0.23][61] 1.3[0.106][61] 0.7[0.16][61] 0.87[0.111][62] 1.0[0.115][62] 1.28[0.12][63] 1.3[0.135][63]	—	—	0.61	3.00	2.44	4.96	5.00

orbitals that are not present in ARPES experiments. This is potentially due to the Fermi surface reconstruction, the origins of which are hotly debated[64, 71, 89]. We take the effective masses directly from figures or values quoted in each publication. These data are divided by the LDA band masses in order to find  $\lambda_{sf}^{dHvA}$  quoted in Table 1.

### c. Specific Heat

Specific-heat measurements determine the mass enhancement by finding the coefficient  $\gamma$  of the electronic specific heat. This is related to the quasiparticle density of states by  $\gamma^*/\gamma = N^*(0)/N(0)$ . The inclusion of additional bands has a possibility of altering our comparisons with the theory, especially for materials where not all bands are due to correlated Cu  $d$ -electrons and con-

tribute to superconductivity, which, *e.g.*, is the case of YBa<sub>2</sub>Cu<sub>3</sub>O<sub>7</sub>. We present  $\lambda_{sf}^{sp.heat}$  in Table 1 by dividing experimental density of states by the LDA determined DOS.

### d. Discrepancies

The discrepancies between photoemission, quantum oscillation, and specific heat measurements can be quite significant. This is seen from our Table 1 and also from Fig. 4 that plots  $\lambda_{sf}$  vs. doping, with various colors referring to various materials and with the shape of the data point denoting a particular experimental technique: ARPES(circles), quantum oscillation (squares), and specific heat (triangles). We also show our calculated  $\lambda_{sf}$  on the vertical axis by arrows following the same color

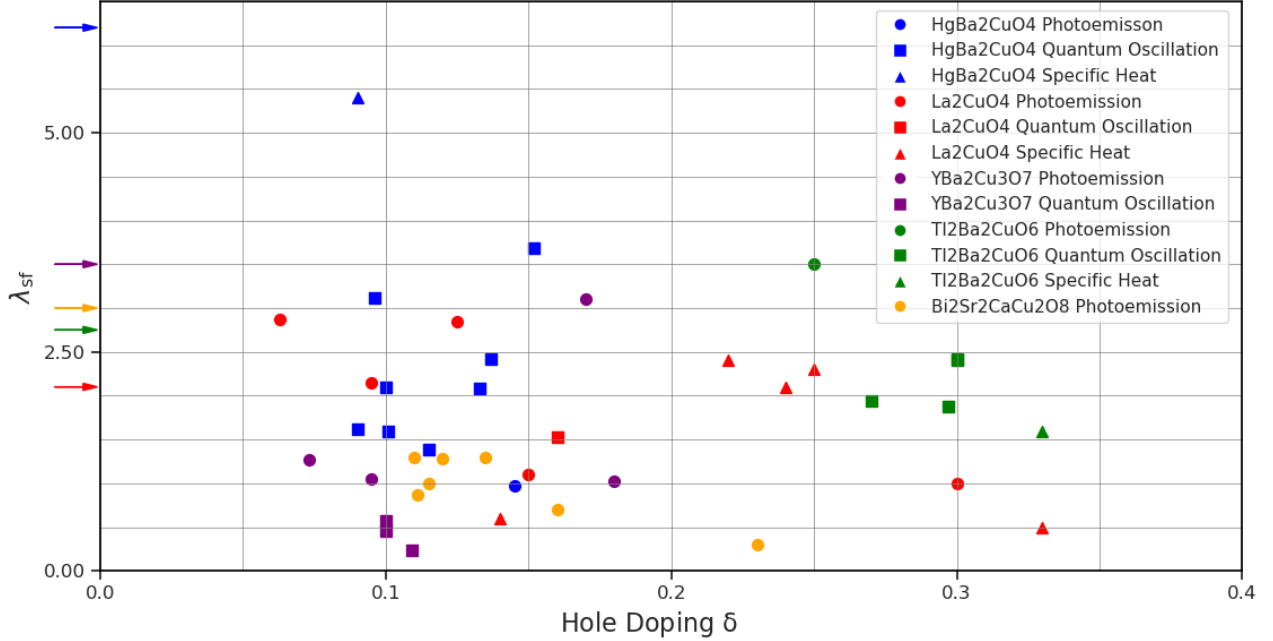


FIG. 4: Experimental mass enhancement parameter  $\lambda_{sf}$  plotted vs doping for several cuprate superconductors studied in this work. Various colors refer to various materials as listed on this figure. The shape of the data point denotes the experimental technique from where  $\lambda_{sf}$  is extracted: ARPES(circles), quantum oscillation (squares), and specific heat (triangles). Theoretically calculated  $\lambda_{sf}$  are shown on the vertical axis by arrows with the color convention as above.

convention. One can generally expect that the mass enhancement is large in the underdoped, strongly correlated regime, but should diminish significantly in the overdoped samples. Unfortunately, this tendency is hard to recognize from the data presented on Fig. 4, although the specific heat data alone (triangles) do point to this trend.

Some quantum oscillation and specific heat measurements have detected a second divergence of the mass enhancement in the cuprate phase diagram[64, 65], near the doping level 0.22 where the pseudogap disappears, but this divergence has not been seen in ARPES. We have omitted these divergent points from Fig.4.

Another question is whether superconductivity competes with or coexists alongside surrounding phases, such as the pseudogap, charge density wave (CDW), and strange metal. This issue remains under debate[72, 90, 91], and the impact of these phases on the experimental extraction of  $\lambda_{sf}$  is not exactly clear. Also, our work does not address any potential ground state competition between these phases and superconductivity.

## V. CONCLUSION

In conclusion, we have studied a series of cuprate superconductors using our recently developed LDA+FLEX(RPA) method that accounts for the

electronic self-energy of the correlated electrons using a summation of the particle-hole bubble and ladder diagrams. Based on this procedure, superconducting energy gaps, Eliashberg spectral functions  $\alpha^2F(\omega)$ , and spin fluctuational coupling constants have been calculated using realistic energy bands, wave functions, and the Fermi surfaces of the cuprates. The Hubbard interaction  $U$  is the only parameter in this method.

The predicted  $d_{x^2-y^2}$  pairing symmetry is a robust feature of our calculation together with the universal shape of the  $\alpha^2F(\omega)$  exhibiting a strong peak at the low-frequency paramagnon region, and its rapid decay towards higher frequencies justifying applicability of the BCS-type approximation. However, a strong dependence on  $U$  of superconducting coupling constant  $\lambda_{\max}$  that comes out as the maximum eigenvalue of the BCS equation, and the same behavior for the calculated quasi-particle mass enhancement  $m^*/m_{LDA} = 1 + \lambda_{sf}$  makes the effective spin fluctuational coupling constant  $\lambda_{eff} = \lambda_{\max}/(1 + \lambda_{sf})$  small unless  $U$  is tuned to be within a few per cent of the SDW instability point that occurs for each material at some  $U_{SDW}$ . This behavior highlighted challenges in building first-principle theories of high-temperature superconductivity but provided a window of opportunity to find the elevated values of  $\lambda_{eff}$  needed to explain the high  $T_c$ 's.

We have also analyzed a wealth of published mass enhancement data that can be extracted from ARPES,

quantum oscillation and specific heat experiments. This data offered additional comparisons with the values of  $\lambda_{sf}$  that we calculated in the hope to find further constraints for the material specific  $U$ 's. Unfortunately, the spread in the experimentally deduced values of  $\lambda_{sf}$  did not offer further insights.

At the end, we hope that gaining further experience with applications of this method and its extensions to other unconventional superconductors will ultimately allow us to reach a more quantitative understanding of unconventional superconductivity in cuprates and other systems.

- 
- [1] K. Miyake, S. Schmitt-Rink, and C. M. Varma, Spin-fluctuation-mediated even-parity pairing in heavy-fermion superconductors, *Phys. Rev. B* **34**, 6554 (1986).
- [2] D. J. Scalapino, E. Loh, J. E. Hirsch,  $d$ -wave pairing near a spin-density-wave instability, *Phys. Rev. B* **34**, 8190 (1986).
- [3] The 1987 Nobel Prize in Physics: J. G. Bednorz and K. A. Müller for their important breakthrough in the discovery of superconductivity in ceramic materials.
- [4] For a review, see, e.g., A.V. Chubukov, D. Pines, J. Schmalian in *The Physics of Conventional and Unconventional Superconductors*, edited by K. H. Bennemann and J. B. Ketterson (Springer-Verlag, 2002).
- [5] H. Shimahara and S. Takada, Superconductivity and Spin Density Wave in Two Dimensional Hubbard Model, *J. Phys. Soc. Japan* **57**, 1044 (1988).
- [6] P. Monthoux, A. V. Balatsky, and D. Pines, Toward a theory of high-temperature superconductivity in the antiferromagnetically correlated cuprate oxides, *Phys. Rev. Lett.* **67**, 3448 (1991).
- [7] K. Kuroki, T. Higashida, and R. Arita, High- $T_c$  superconductivity due to coexisting wide and narrow bands: A fluctuation exchange study of the Hubbard ladder as a test case, *Phys. Rev. B* **72**, 212509 (2005).
- [8] T. Takimoto, T. Hotta, and K. Ueda, Strong-coupling theory of superconductivity in a degenerate Hubbard model, *Phys. Rev. B* **69**, 104504, (2004).
- [9] N. Kitamine, M. Ochi, K. Kuroki, Designing nickelate superconductors with  $d^8$  configuration exploiting mixed-anion strategy, *Phys. Rev. Res.* **2**, 042032 (2020).
- [10] Y. Zhang, L.-F. Lin, A. Moreo, T. Maier, E. Dagotto, Structural phase transition,  $s_{\pm}$ -wave pairing, and magnetic stripe order in bilayered superconductor  $\text{La}_3\text{Ni}_2\text{O}_7$  under pressure, *Nature Comm.* **15**, 2470 (2024).
- [11] I. I. Mazin, D. J. Singh, Ferromagnetic Spin Fluctuation Induced Superconductivity in  $\text{Sr}_2\text{RuO}_4$ , *Phys. Rev. Lett.* **79**, 733 (1997).
- [12] T. Takimoto, Orbital fluctuation-induced triplet superconductivity: Mechanism of superconductivity in  $\text{Sr}_2\text{RuO}_4$ , *Phys. Rev. B* **62**, R14641 (2000).
- [13] K. Yada, H. Kontani, Origin of Weak Pseudogap Behaviors in  $\text{Na}_{0.35}\text{CoO}_2$ : Absence of Small Hole Pockets, *J. Phys. Soc. Japan* **74**, 2161 (2005).
- [14] H. Ikeda, Pseudogap and Superconductivity in Iron-Based Layered Superconductor Studied by Fluctuation-Exchange Approximation, *Journal of the Phys. Soc. of Japan* **77**, 123707 (2008).
- [15] J. Zhang, R. Sknepnek and J. Schmalian, Spectral analysis for the iron-based superconductors: Anisotropic spin fluctuations and fully gapped  $s_{\pm}$ -wave superconductivity, *Phys. Rev. B* **82**, 134527 (2010).
- [16] Z.-J. Yao, J.-X. Li, and Z. D. Wang, Spin fluctuations, interband coupling and unconventional pairing in iron-based superconductors, *New J. of Physics* **11**, 2 (2009).
- [17] S. Graser, and T. Kemper, T. A. Maier, H.-P. Cheng, P. J. Hirschfeld, D. J. Scalapino, Spin fluctuations and superconductivity in a three-dimensional tight-binding model for  $\text{BaFe}_2\text{As}_2$ , *Phys. Rev. B* **81**, 214503 (2010).
- [18] T. Takimoto, T. Hotta, K. Ueda, Strong-coupling theory of superconductivity in a degenerate Hubbard model, *Phys. Rev. B* **69**, 104504 (2004).
- [19] Y. Yanase, M. Sgrist, Superconductivity and Magnetism in Non-centrosymmetric System: Application to  $\text{CePt}_3\text{Si}$ , *J. Phys. Soc. Japan* **77**, 124711 (2008).
- [20] For a review, see, e.g., *Theory of the Inhomogeneous Electron Gas*, edited by S. Lundqvist and S. H. March (Plenum, New York, 1983).
- [21] N. E. Bickers, D. J. Scalapino and S. R. White, Conserving Approximations for Strongly Correlated Electron Systems: Bethe-Salpeter Equation and Dynamics for the Two-Dimensional Hubbard Model, *Phys. Rev. Lett.* **62**, 961 (1989).
- [22] S. Doniach and S. Engelsberg, Low-Temperature Properties of Nearly Ferromagnetic Fermi Liquids, *Phys. Rev. Lett.* **17**, 750 (1966).
- [23] N. F. Berk and J. R. Schrieffer, Effect of Ferromagnetic Spin Correlations on Superconductivity, *Phys. Rev. Lett.* **17**, 433 (1966).
- [24] B. Menge and E. Mueller-Hartmann, The Hubbard model at high dimensions: self-consistent weak coupling theory, *Z. Phys. B: Cond. Mat.* **82**, 237 (1991).
- [25] For a review, see, e.g., Y. Yanase, T. Jujo, T. Nomura, H. Ikeda, T. Hotta, K. Yamada, Theory of superconductivity in strongly correlated electron systems, *Phys. Reports* **387**, 1 (2003).
- [26] M. Kitatani, N. Tsuji, H. Aoki, FLEX+DMFT approach to the  $d$ -wave superconducting phase diagram of the two-dimensional Hubbard model, *Phys. Rev. B* **92**, 8, (2015).
- [27] T. A. Maier, M. Jarrell, and D. J. Scalapino, Pairing interaction in the two-dimensional Hubbard model studied with a dynamic cluster quantum Monte Carlo approximation, *Phys. Rev. B* **74**, 094513 (2006).
- [28] P. Mai, G. Balduzzi, S. Johnston, and T. A. Maier, Pairing correlations in the cuprates: A numerical study of the three-band Hubbard model, *Phys. Rev. B* **103**, 144514 (2021).
- [29] V. I. Anisimov, J. Zaanen, and O. K. Andersen, Band theory and Mott insulators: Hubbard  $U$  instead of Stoner  $I$ , *Phys. Rev. B* **44**, 943 (1991).
- [30] For a review, see, e.g., G. Kotliar, S. Y. Savrasov, K. Haule, V. S. Oudovenko, O. Parcollet, C.A. Marianetti, Electronic structure calculations with dynamical mean-field theory, *Rev. Mod. Phys.* **78**, 865, (2006).
- [31] S. Y. Savrasov, G. Resta, X. Wan, Local self-energies for V and Pd emergent from a nonlocal LDA+FLEX implementation, *Phys. Rev. B* **97**, 155128 (2018).
- [32] G. Heier, S. Y. Savrasov, Calculated spin fluctuational pairing interaction in  $\text{HgBa}_2\text{CuO}_4$  using LDA+FLEX method, *Phys. Rev. B* **109**, 094506 (2024).
- [33] G. Heier, K. Park, S. Y. Savrasov, Competing  $d_{xy}$  and

- $s_{\pm}$  Pairing Symmetries in Superconducting  $\text{La}_3\text{Ni}_2\text{O}_7$ : LDA+FLEX Calculation, Phys. Rev. B **109**, 104508 (2024).
- [34] Y. Tian and S. Y. Savrasov, Calculated Unconventional Superconductivity via Charge Fluctuations in Kagome Metal  $\text{CsV}_3\text{Sb}_5$ , arXiv:2405.03137.
- [35] J. Bardeen, L.N. Cooper, J.R. Schrieffer, Theory of Superconductivity, Phys. Rev. **108**, 1175 (1957).
- [36] W. L. McMillan, Transition Temperature of Strong-Coupled Superconductors, Phys. Rev. **167**, 331 (1968).
- [37] M. A. L. Marques, M. Lüders, N. N. Lathiotakis, G. Profeta, A. Floris, L. Fast, A. Continenza, E. K. U. Gross, and S. Massidda, Ab initio theory of superconductivity. II. Application to elemental metals, Phys. Rev. B **72**, 024546 (2005).
- [38] R. Arita, K. Kuroki and H. Aoki,  $d$ - and  $p$ -Wave Superconductivity Mediated by Spin Fluctuations in Two- and Three-Dimensional Single-Band Repulsive Hubbard Model, J. Phys. Soc. Japan **69**, 1181 (2000).
- [39] S. N. Putilin, E. V. Antipov, O. Chmaissem and M. Marezio, Superconductivity at 94 K in  $\text{HgBa}_2\text{CuO}_{4+x}$ , Nature **362**, 226 (1993).
- [40] Q. Q. Liu, X. M. Qin, Y. Yu, F. Y. Li, C. Dong, C. Q. Jin, High pressure synthesis of a new superconductor  $\text{Sr}_2\text{CuO}_{2+\delta}\text{Cl}_{2-y}$  induced by “apical oxygen doping”, Physica C: Superconductivity **420**, 23 (2005).
- [41] C. C. Torardi, M. A. Subramanian, J. C. Calabrese, J. Gopalakrishnan, E. M. McCarron, K. J. Morrissey, T. R. Askew, R. B. Flippen, U. Chowdhry, and A. W. Sleight, Structures of the superconducting oxides  $\text{Tl}_2\text{Ba}_2\text{CuO}_6$  and  $\text{Bi}_2\text{Sr}_2\text{CuO}_6$ , Phys. Rev. B **38**, 225 (1988).
- [42] J. G. Bednorz and K. A. Müller, Possible High- $T_c$  Superconductivity in Ba-La-Cu-O system, Z. Phys. B - Condensed Matter **64**, 189 (1986).
- [43] J. H. Schön, M. Dorget, F. C. Beuran, X. Z. Zu, E. Arushanov, C. Deville Cavellin & M. Laguës, Superconductivity in  $\text{CaCuO}_2$  as a result of field-effect doping, Nature **414**, 434 (2001).
- [44] M. K. Wu, J. R. Ashburn, C. J. Torng, P. H. Hor, R. L. Meng, L. Gao, Z.J. Huang, Y.Q. Wang, C.W. Chu, Superconductivity at 93 K in a New Mixed-Phase Y-Ba-Cu-O Compound System at Ambient Pressure, Phys. Rev. Lett. **58**, 908 (1988).
- [45] Z. Z. Sheng and A. M. Hermann, Bulk superconductivity at 120 K in the Tl-Ca/Ba-Cu-O system, Nature **332**, 138 (1988).
- [46] H. Maeda, Y. Tanaka, M. Fukutomi, T. Asano, A New High- $T_c$  Oxide Superconductor without a Rare Earth Element, Japanese Journal of Applied Physics **27**, 209 (1988).
- [47] For a review, see, e.g., M. Fujita, H. Hiraka, M. Matsuda, M. Matsuura, J. M. Tranquada, S. Wakimoto, G. Xu, and K. Yamada, Progress in Neutron Scattering Studies of Spin Excitations in High- $T_c$  Cuprates, J. Phys. Soc. Japan **81**, 011007 (2012).
- [48] H. A. Mook, M. Yethiraj, G. Aeppli, T. E. Mason, and T. Armstrong, Polarized neutron determination of the magnetic excitations in  $\text{YBa}_2\text{Cu}_3\text{O}_7$ , Phys. Rev. Lett. **70**, 3490 (1993).
- [49] For a review, see, e.g., A. Damascelli, Z. Hussain, and Z.-X. Shen, Angle-resolved photoemission studies of the cuprate superconductors, Rev. Mod. Phys. **75**, 473 (2003).
- [50] S. Teranishi, K. Nishiguchi, K. Kusakabe, Material-Dependent Screening of Coulomb Interaction in Single-Layer Cuprates, J. Phys. Soc. Japan **87**, 114701 (2018).
- [51] J.-B. Moree, M. Hirayama, M. T. Schmid, Y. Yamaji, M. Imada, Ab initio low-energy effective Hamiltonians for the high-temperature superconducting cuprates  $\text{Bi}_2\text{Sr}_2\text{CuO}_6$ ,  $\text{Bi}_2\text{Sr}_2\text{CaCu}_2\text{O}_8$ ,  $\text{HgBa}_2\text{CuO}_4$ , and  $\text{CaCuO}_2$ , Phys. Rev. B **106**, 235150 (2022).
- [52] I. M. Vishik, N. Bari, M. K. Chan, Y. Li, D. D. Xia, G. Yu, X. Zhao, W.S. Lee, W. Meevasana, T. P. Devereaux, M. Greven, Z.-X. Shen, Angle-resolved photoemission spectroscopy study of  $\text{HgBa}_2\text{CuO}_{4+\delta}$ , Phys. Rev. B **89**, 195141 (2014).
- [53] B. O. Wells, Z. -X. Shen, A. Matsuura, D. M. King, M. A. Kastner, M. Greven, R. J. Birgeneau,  $E$  versus  $k$  Relations and Many Body Effects in the Model Insulating Copper Oxide  $\text{Sr}_2\text{CuO}_2\text{Cl}_2$ , Phys. Rev. Lett. **74**, 964 (1995).
- [54] D. C. Peets, J.D.F. Mottershead, B. Wu, I. S. Elfimov, R. Liang, W.N. Hardy, D.A. Bonn, M. Raudsepp, N.J.C. Ingle, A. Damascelli,  $\text{Tl}_2\text{Ba}_2\text{CuO}_{6+\delta}$  brings spectroscopic probes deep into the overdoped regime of the high- $T_c$  cuprates, New Journal of Physics **9**, 28 (2007).
- [55] T. Valla, T. E. Kidd, W.-G. Yin, G. D. Gu, P. D. Johnson, Z.-H. Pan, and A. V. Fedorov, High-Energy Kink Observed in the Electron Dispersion of High-Temperature Cuprate Superconductors, Phys. Rev. Lett. **98**, 167003 (2007).
- [56] A. Ino, C. Kim, M. Nakamura, T. Yoshida, T. Mizokawa, A. Fujimori, A. Z.-X. Shen, T. Kakeshita, H. Eisaki, S. Uchida, Doping-dependent evolution of the electronic structure of  $\text{La}_{2-x}\text{Sr}_x\text{CuO}_4$  in the superconducting and metallic phases, Phys. Rev. B **65**, 094504 (2002).
- [57] A. Kaminski, H. M. Fretwell, M. R. Norman, M. Randeria, S. Rosenkranz, U. Chatterjee, J. C. Campuzano, J. Mesot, T. Sato, T. Takahashi, T. Terashima, M. Takano, K. Kadowaki, Z. Z. Li, H. Raffy, H., Momentum anisotropy of the scattering rate in cuprate superconductors, Phys. Rev. B **71**, 014517 (2005).
- [58] S. V. Borisenko, A. A. Kordyuk, V. Zabolotnyy, J. Geck, D. Inosov, A. Koitzsch, J. Fink, M. Knupfer, B. Buechner, V. Hinkov, C. T. Lin, B. Keimer, T. Wolf, S. G. Chizbaafian, L. Patthey, R. Follath, Kinks, Nodal Bilayer Splitting, and Interband Scattering in  $\text{YBa}_2\text{Cu}_3\text{O}_{6+x}$ , Phys. Rev. Lett. **96**, 117004 (2006).
- [59] A. Junod and A. Bezing and J. Müller, Optimization of the specific heat jump at  $T_c$  and magnetic properties of the superconductor  $\text{YBa}_2\text{Cu}_3\text{O}_7$ , Physica C: Superconductivity **152**, 50 (1988).
- [60] W. S. Lee, K. Tanaka, I. M. Vishik, D. H. Lu, R. G. Moore, H. Eisaki, A. Iyo, T. P. Devereaux, Z. X. Shen, Dependence of Band-Renormalization Effects on the Number of Copper Oxide Layers in Tl-Based Copper Oxide Superconductors Revealed by Angle-Resolved Photoemission Spectroscopy, Phys. Rev. Lett. **103**, 067003 (2009).
- [61] Y. Zhong, Y. Wang, S. Han, Y.-F. Lv, W.-L. Wang, D. Zhang, H. Ding, Y.-M. Zhang, L. Wang, K. He, R. Zhong, J. A. Schneeloch, G.-D. Gu, C.-L. Song, X.-C. Ma, Q.-K. Xue, Nodeless pairing in superconducting copper-oxide monolayer films on  $\text{Bi}_2\text{Sr}_2\text{CaCu}_2\text{O}_{8+\delta}$ , Science Bulletin **61**, 1239 (2016).
- [62] A.A. Kordyuk and S.V. Borisenko and A. Koitzsch and J. Fink and M. Knupfer and B. Bachner and H. Berger, Life of the nodal quasiparticles in Bi-2212 as seen by

- ARPES, *J. Phys. Chem. of Solids* **67**, 201 (2006).
- [63] P. V. Bogdanov, A. Lanzara, S. A. Kellar, X. J. Zhou, E. D. Lu, W. J. Zheng, G. Gu, J.-I. Shimoyama, K. Kishio, H. Ikeda, R. Yoshizaki, Z. Hussain, Z.X. Shen, Evidence for an Energy Scale for Quasiparticle Dispersion in  $\text{Bi}_2\text{Sr}_2\text{CaCu}_2\text{O}_8$ , *Phys. Rev. Lett.* **85**, 2581 (2000).
- [64] M. K. Chan, R. D. McDonald, B. J. Ramshaw, J. B. Betts, A. Shekhter, E. D. Bauer, N. Harrison, Extent of Fermi-surface reconstruction in the high-temperature superconductor  $\text{HgBa}_2\text{CuO}_{4+\delta}$ , *Proc. of Nat. Acad. of Sciences* **117**, 9782 (2020).
- [65] N. B Barisc, M. K. Chan, C. T. Dorow, Wojciech, B. Vignolle, Baptiste, G. Yu, J. Beard, X. Zhao, C. Proust, M. Greven, Martin, Universal quantum oscillations in the underdoped cuprate superconductors, *Nature Phys.* **9**, 761 (2013).
- [66] M. K. Chan, N. Harrison, R. D. McDonald, B. J. Ramshaw, K. A. Modic, N. Baris, M. Greven, Single reconstructed Fermi surface pocket in an underdoped single-layer cuprate superconductor, *Nature Comm.* **7**, 12244 (2016).
- [67] A. F. Bangura, P. M. C. Rourke, T. M. Benseman, M. Matusiak, J. R. Cooper, N. E. Hussey, A. Carrington, Fermi surface and electronic homogeneity of the overdoped cuprate superconductor  $\text{Tl}_2\text{Ba}_2\text{CuO}_{6+\delta}$  as revealed by quantum oscillations, *Phys. Rev. B* **82**, 140501 (2010).
- [68] J. A. Wilson, Elucidation of the origins of transport behaviour and quantum oscillations in high temperature superconducting cuprates, *J. Phys.: Cond. Mat.* **21**, 245702 (2009).
- [69] K. W. Post, A. Legros, D.G. Rickel, J. Singleton, R. D. McDonald, X. He, I. Bo, X. Xu, X. Shi, N.P. Armitage, S.A. Crooker, Observation of cyclotron resonance and measurement of the hole mass in optimally doped  $\text{La}_{2-x}\text{Sr}_x\text{CuO}_4$ , *Phys. Rev. B* **103**, 134515 (2021).
- [70] C. Jaudet, D. A. Bonn, W. N. Hardy, L. Taillefer, C. Proust, de Haas-van Alphen Oscillations in the Underdoped High-Temperature Superconductor  $\text{YBa}_2\text{Cu}_3\text{O}_{6.5}$ , *Phys. Rev Lett.* **100**, 18 (2008).
- [71] N. Doiron-Leyraud L. Taillefer and et al., Quantum oscillations and the Fermi surface in an underdoped high- $T_c$  superconductor, *Nature* **447**, 565 (2007).
- [72] J. Kak, I. Vinograd, B. Michon, A. Rydh, A. Demuer, R. Zhou, H. Mayaffre, R. Liang, W.N. Hardy, D.A. Bonn, and N. Doiron-Leyraud, L. Taillefer, M.-H. Julien, C. Marcenat, T. Klein, T., Unusual Interplay between Superconductivity and Field-Induced Charge Order in  $\text{YBa}_2\text{Cu}_3\text{O}_y$ , *Phys. Rev. Lett.* **121**, 167002 (2018).
- [73] C. Girod, A. Legros, A. Forget, D. Colson, C. Marcenat, A. Demuer, D. LeBoeuf, L. Taillefer, T. Klein, High density of states in the pseudogap phase of the cuprate superconductor  $\text{HgBa}_2\text{CuO}_{4+\delta}$  from low-temperature normal-state specific heat, *Phys. Rev. B* **102**, 014506 (2020).
- [74] J.M. Wade, J.W. Loram, K.A. Mirza, J. R. Cooper, J.L. Tallon, Electronic specific heat of  $\text{Tl}_2\text{Ba}_2\text{CuO}_{6+\delta}$  from 2 K to 300 K for  $0 \leq \delta \leq 0.1$ , *J. Supercond.* **7**, 261 (1994).
- [75] S. Nakamae, K. Behnia, N. Mangkorntong, N. Nohara, H. Takagi, S.J.C. Yates, N.E. Hussey, Electronic ground state of heavily overdoped nonsuperconducting  $\text{La}_{2-x}\text{Sr}_x\text{CuO}_4$ , *Phys. Rev. B* **68**, 100502 (2003).
- [76] B. Michon, C. Girod, S. Badoux, J. Kacmarcik, Q. Ma, M. Dragomir, H. A. Dabkowska, B. D. Gaulin, J.-S. Zhou, S. Pyon, T. Takayama, H. Takagi, S. Verret, N. Doiron-Leyraud, C. Marcenat, L. Taillefer, T. Klein, Thermodynamic signatures of quantum criticality in cuprate superconductors, *Nature* **567**, 218 (2019).
- [77] H. A. Mook, M. Yethiraj, G. Aeppli, T. E. Mason, T. Armstrong, Polarized neutron determination of the magnetic excitations in  $\text{YBa}_2\text{Cu}_3\text{O}_7$ , *Phys. Rev. Lett.* **70**, 3490 (1993).
- [78] M. Fujita, H. Hiraka, M. Matsuda, M. Masaki, J. Tranquada, S. Wakimoto, G. Xu, K. Yamada, Progress in Neutron Scattering Studies of Spin Excitations in High- $T_c$  Cuprates, *J. Phys. Soc. Japan* **81**, 011007 (2012).
- [79] A. S. Alexandrov, Unconventional pairing symmetry of layered superconductors caused by acoustic phonons, *Phys. Rev. B* **77**, 094502, (2008).
- [80] S. Y. Savrasov, Linear-response theory and lattice dynamics: A muffin-tin-orbital approach, *Phys. Rev. B* **54**, 16470 (1996).
- [81] A. Lanzara, P. V. Bogdanov, X. J. Zhou, S. A. Kellar, D. L. Feng, E. D. Lu, T. Yoshida, H. Eisaki, A. Fujimori, K. Kishio, J.-I. Shimoyama, T. Noda, S. Uchida, Z. Hussain, Z.-X. Shen, Evidence for ubiquitous strong electron-phonon coupling in high-temperature superconductors, *Nature* **412**, 510 (2001).
- [82] S. Y. Savrasov and O. K. Andersen, Linear-Response Calculation of the Electron-Phonon Coupling in Doped  $\text{CaCuO}_2$ , *Phys. Rev. Lett.* **77**, 4430 (1996).
- [83] F. Giustino, M. L. Cohen and S. G. Louie, Small phonon contribution to the photoemission kink in the copper oxide superconductors, *Nature* **452**, 975 (2008).
- [84] H. A. Mook, M. Yethiraj, G. Aeppli, T. E. Mason, T., Armstrong, Polarized neutron determination of the magnetic excitations in  $\text{YBa}_2\text{Cu}_3\text{O}_7$ , *Phys. Rev. Lett.* **70**, 3490 (1993).
- [85] T. Maier, T. Berlijn, D. J. Scalapino, Two pairing domes as  $\text{Cu}^{2+}$  varies to  $\text{Cu}^{3+}$ , *Phys. Rev. B* **99**, 224515 (2019).
- [86] T. A. Maier, A. Macridin, M. Jarrell, and D. J. Scalapino, Systematic analysis of a spin-susceptibility representation of the pairing interaction in the two-dimensional Hubbard model, *Phys. Rev. B* **76**, 144516 (2007).
- [87] K. Tamasaku, Y. Nakamura, S. Uchida, Charge dynamics across the  $\text{CuO}_2$  planes in  $\text{La}_{2-x}\text{Sr}_x\text{CuO}_4$ , *Phys. Rev. Lett.* **69**, 1455 (1992).
- [88] B. J. Ramshaw, S. E. Sebastian, R. D. McDonald, James Day, B. S. Tan, Z. Zhu, J. B. Betts, R. Liang, D. A. Bonn, W. N. Hardy, N. Harrison, Quasiparticle mass enhancement approaching optimal doping in a high- $T_c$  superconductor, *Science* **348**, 317 (2015).
- [89] T. Das, Electron-like Fermi surface and in-plane anisotropy due to chain states in  $\text{YBa}_2\text{Cu}_3\text{O}_{7-\delta}$  superconductors, *Phys. Rev. B* **86**, 064527 (2012).
- [90] J. Meng, W. Zhang, G. Liu, L. Zhao, H. Liu, X. Jia, W. Lu, X. Dong, G. Wang, H. Zhang, Y. Zhou, Y. Zhu, X. Wang, Z. Zhao, Z. Xu, C. Chen, X.J. Zhou, Monotonic,  $d$ -wave superconducting gap of the optimally doped  $\text{Bi}_2\text{Sr}_{1.6}\text{La}_{0.4}\text{CuO}_6$  superconductor by laser-based angle-resolved photoemission spectroscopy, *Phys. Rev. B* **79**, 024514 (2009).
- [91] T. K. Kondo, T. Rustem, T. Takeuchi, J. Schmalian, A. Kaminski, Competition between the pseudogap and superconductivity in the high- $T_c$  copper oxides, *Nature* **457**, 296 (2009).